Biophysical Chemistry 184 (2013) 44–53

Contents lists available at ScienceDirect

Biophysical Chemistry

journal homepage: http://www.elsevier.com/locate/biophyschem

Structural studies of the *Trypanosoma cruzi* Old Yellow Enzyme: Insights into enzyme dynamics and specificity

Mário T. Murakami [a,1], Nathalia C. Rodrigues [b,1], Lisandra M. Gava [c], Rodrigo V. Honorato [a], Fernanda Canduri [d], Leandro R.S. Barbosa [e], Glaucius Oliva [b], Júlio C. Borges [d,*]

[a] *Laboratório Nacional de Biociências - LNBio/CNPEM-ABTLuS, Campinas, SP 13083-970, Brazil*
[b] *Instituto de Física de São Carlos, USP, São Carlos, SP 13566-590, Brazil*
[c] *Departamento de Genética e Evolução, Universidade Federal de São Carlos, São Carlos, SP 13565-905, Brazil*
[d] *Instituto de Química de São Carlos, USP, São Carlos, SP 13560-970, Brazil*
[e] *Instituto de Física, USP, São Paulo, SP 05508-090, Brazil*

HIGHLIGHTS

- The high-resolution crystallographic structure of TcOYE was solved at 1.27 Å resolution.
- It has a classical $(\alpha/\beta)_8$ fold with the FMN prosthetic group bound to a deep cleft.
- In solution, TcOYE is a monomer and displays a distinct conformational state compared to the crystal structure due to long and flexible loops.
- Molecular dynamics shed light in the interaction mechanism with three naphthoquinones.

GRAPHICAL ABSTRACT

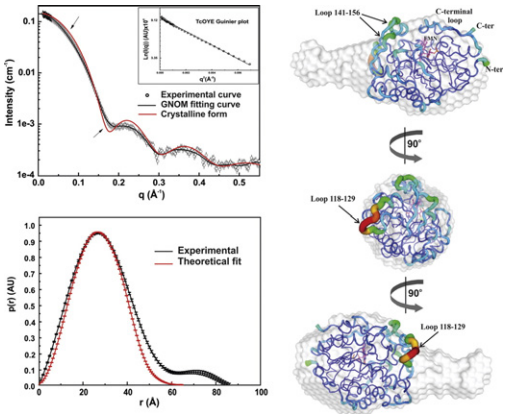

ARTICLE INFO

Article history:
Received 26 July 2013
Received in revised form 12 August 2013
Accepted 12 August 2013
Available online 28 August 2013

Keywords:
OYE
Trypanosoma cruzi
Chagas disease
Crystal structure
SAXS
Protein dynamics

ABSTRACT

The flavoprotein old yellow enzyme of *Trypanosoma cruzi* (TcOYE) is an oxidoreductase that uses NAD(P)H as co-factor. This enzyme is clinically relevant due to its role in the action mechanism of some trypanocidal drugs used in the treatment of Chagas' disease by producing reactive oxygen species. In this work, the recombinant enzyme TcOYE was produced and collectively, X-ray crystallography, small angle X-ray scattering, analytical ultracentrifugation and molecular dynamics provided a detailed description of its structure, specificity and hydrodynamic behavior. The crystallographic structure at 1.27 Å showed a classical $(\alpha/\beta)_8$ fold with the FMN prosthetic group buried at the positively-charged active-site cleft. In solution, TcOYE behaved as a globular monomer, but it exhibited a molecular envelope larger than that observed in the crystal structure, suggesting intrinsic protein flexibility. Moreover, the binding mode of β-lapachone, a trypanocidal agent, and other naphthoquinones was investigated by molecular docking and dynamics suggesting that their binding to TcOYE are stabilized mainly by interactions with the isoalloxazine ring from FMN and residues from the active-site pocket.

Abbreviations: AUC, analytical ultracentrifugation; CD, circular dichroism; D_{max}, maximum distance; f/f_0, frictional ratio; MM, molecular mass; R_s, Stokes radius; R_g, radius of gyration; $s_{20,w}$, sedimentation coefficient at standard conditions; $s^0_{20,w}$, standard sedimentation coefficient at 0 mg mL^{-1} of protein; [Θ], mean residue ellipticity.

* Corresponding author at: Instituto de Química de São Carlos, Universidade de São Paulo, USP, P.O. Box 780, Zip Code 13560-970, São Carlos, SP, Brazil. Tel.: +55 16 3373 8637; fax: +55 16 3373 9982.
E-mail address: borgesjc@iqsc.usp.br (J.C. Borges).

[1] Both authors have equally contributed to this work.

0301-4622/$ – see front matter © 2013 Elsevier B.V. All rights reserved.
http://dx.doi.org/10.1016/j.bpc.2013.08.004

1. Introduction

Chagas' disease is caused by the protozoan *Trypanosoma cruzi* and represents a still serious public health problem in developing countries throughout South and Central America, with nearly 8 million people infected while 28 million are at risk of infection [1]. This disease leads to severe acute and chronic complications, which may compromise the economic life of the patient [1]. Nifurtimox and benznidazole are the current drug treatments for this disease, which act by forming free radical anions and reactive oxygen species. However, these drugs have limited efficacy and often provoke harmful side effects [1]. In addition, several cases have been reported for the resistance of *T. cruzi* to these compounds [1–3]. The current scenario highlights the importance of studies on the development of new and more effective drugs against *T. cruzi*. Consequently, efforts to elucidate the action mechanism of new potential molecular targets for rational drug design strategies have been conducted by several groups (reviewed in [2,4]).

It was recently shown that the enzyme prostaglandin F2α synthase, which reduces the 9,11-endoperoxide PGH2 to PGF2α, is responsible for the drug-metabolizing activity of trypanocidal drugs, such as nifurtimox, benznidazole and the diterpene komaroviquinone in *T. cruzi* [5,6]. This enzyme is also called *T. cruzi* Old Yellow Enzyme (TcOYE) due to the presence of its flavin mononucleotide prosthetic group [6], which gives its characteristic coloring. The oxidoreductase activity of TcOYE is dependent of NAD(P)H that acts as cofactor. Its drug-metabolizing activity has been suggested by the TcOYE over-expression in *T. cruzi* strains susceptible to benznidazole [7] and by the *T. cruzi* benznidazole resistance when TcOYE gene copies were deleted [8]. Moreover, TcOYE immunoprecipitation from *T. cruzi* cell lysates abolished, under anaerobic conditions, the reductase activity for peroxides, naphthoquinones and nitroheterocyclic drugs supporting the role of TcOYE in drug metabolism [6].

Despite the importance of TcOYE in trypanocidal drugs and prostaglandin metabolism [6], few studies detailing its structure in solution have been reported [9,10]. In this work, we have produced the recombinant TcOYE isoform from *T. cruzi* 17WTS strain and investigated its structural and dynamics properties by X-ray crystallography, small angle X-ray scattering, analytical ultracentrifugation and molecular dynamics. The holoenzyme structure was solved in two crystalline forms at 1.27 and 2.00 Å resolution and SAXS data pointed out that TcOYE displayed some intrinsic flexibility related to interfacial loops with high B-factors. TcOYE molecular docking studies with naphthoquinone compounds, like β-lapachone, a natural compound [11] that is metabolized by TcOYE into a semiquinone radical anion, suggested the TcOYE binding mode. All tested ligands seem to make hydrophobic interactions with the FMN isoalloxazine ring and Phe^{71} and Met^{290} residues as well as hydrogen bonds with Thr^{28}, His^{195} and Tyr^{200}.

2. Material and methods

2.1. Cloning, expression and purification

The genomic DNA from *T. cruzi* 17WTS strain was used as template to amplify the DNA sequence of TcOYE (GenBank ID: 61741940) with the following primers 5′-TTTCATATGGCGACGTTCCCTG-3′ and 5′-GAGGTATCAAGCTTATTTGTTGTACG-3′. The amplified DNA was cloned into the pET28a expression vector (Novagen) yielding TcOYE with a His-tag fused to its N-terminal (His-TcOYE). The cloning process was checked by automated DNA sequencing. The recombinant protein was expressed in *E. coli* BL21(DE3) strain, at 30 °C, in LB medium containing 30 μg mL^{-1} of kanamycin. The cells were grown to an optical density at 600 nm of 0.4, with addition of 0.1 mM of isopropyl thio-β-D-galactoside. After 4 h of induction, the cells were harvested by centrifugation at 2600 ×*g* for 10 min. The cells were disrupted by sonication, after incubation for 30 min on ice with 5 U of DNAse (Promega) and 30 μg mL^{-1} of lysozyme (Sigma), and centrifuged 2 times at 20,000 ×*g* for 30 min at 4 °C. The supernatant was submitted to affinity chromatography in a HiTrap Chelating column (GE Healthcare) coupled to an ÄKTA Prime system (GE Healthcare) equilibrated with 20 mM phosphate (pH 7.5) with 500 mM NaCl. The bound fractions were eluted with 500 mM imidazole solved in the aforementioned buffer. The His-tag was released from the His-TcOYE by incubating of 10–15 mg of protein with 10 U of thrombin (Sigma) at 4 °C for 24 h; after the incubation time the noncleaved His-tagged protein was separated by nickel affinity chromatography. The cleaved protein (named TcOYE) was loaded onto a HiLoad Superdex 200 pg 16/60 size exclusion column (GE Healthcare) equilibrated with 25 mM Tris–HCl (pH 8.0) containing 100 mM NaCl and 1 mM β-mercaptoethanol. The efficacy of each purification step was assessed by 12% SDS-PAGE. The protein concentration was determined by UV absorbance at 280 nm, using the calculated extinction coefficient of 64,600 M^{-1} cm^{-1}, calculated at water conditions by the Sednterp program (www.jphilo.mailway.com/download.htm) using the TcOYE amino acid sequence, and summing the FMN extinction coefficient at 280 nm.

2.2. Circular dichroism spectroscopy

Circular dichroism (CD) measurements were performed in a Jasco J-815 spectropolarimeter connected to a Peltier-type temperature control system PFD 425S. The TcOYE was tested in 25 mM Tris–HCl (pH 8.0) containing 100 mM NaCl and 1 mM β-mercaptoethanol, at 4 different molar concentrations ranging from 2 to 25 μM in a 0.2 and 1.0 mm pathlength Hellma cuvette. The CD spectra were normalized to residual molar ellipticity ([Θ]) and averaged.

2.3. Crystallization

Crystallization experiments were performed at 292 K by the hanging-drop vapor diffusion method. Typically, 2 μL of protein solution at 14 mg mL^{-1} in 25 mM Tris–HCl (pH 8.0) containing 100 mM NaCl and 1 mM β-mercaptoethanol was mixed with an equal volume of the reservoir solution and equilibrated against 0.5 mL of reservoir solution. The better-quality crystals grew within 10 days from a condition containing 28% ($w\ v^{-1}$) polyethylene glycol 1500 and 0.3 M ammonium fluoride.

2.4. Data collection and processing

A single crystal was harvested using a nylon loop (Hampton Research) and transferred from the crystallization drop to a fresh 2 μL cryo-solution containing 10% glycerol, 28% PEG 1500 and 0.3 M ammonium fluoride. The crystal was then flash-cooled to 100 K in a nitrogen gas stream in order to prevent radiation damage during data collection. Data sets were collected on the MX2 beamline at the Brazilian Synchrotron Light Laboratory (Campinas, Brazil) using a MARMOSAIC 225 detector to record the intensities. Depending on crystal symmetry, different data collection strategies were adopted in order to optimize oscillation range, oscillation per frame, sample-to-detector distance and exposure time. The data were indexed, integrated and scaled using the HKL2000 package [12].

2.5. Structure determination and refinement

The structure was solved by molecular replacement using the *Molrep* program [13] and the atomic coordinates of TcOYE isoform (PDB code: 3ATY) [9]. The refinement was performed by using the REFMAC5 program as implemented in the *CCP*4 program suite [14]. The electron density maps were examined and model building was carried out using the *COOT* program [15]. The final model was analyzed using the *MOLPROBITY* program [16]. The atomic coordinates and structure factors of the TcOYE structure in $P2_12_12_1$ and $P2_1$ crystalline forms have

been deposited in the Protein Data Bank with the accession codes 4E2B and 4E2D, respectively.

2.6. Analytical size-exclusion chromatography

The Superdex 200 GL 10/300 column (GE Healthcare) coupled to an ÄKTA Prime device (GE Healthcare) equilibrated with 25 mM Tris–HCl (pH 8.0), NaCl 100 mM, containing 1 mM β-mercaptoethanol was used to carry out analytical size exclusion chromatography (aSEC) experiments in a flow rate of 0.5 mL min^{-1}. The column was calibrated with standard proteins of known Stokes radii (R_s): apoferritin (67 Å); γ-globulin (48 Å), bovine serum albumin (36 Å), ovalbumin (30 Å), carbonic anhydrase (24 Å) and cytochrome c (14 Å) with absorbance monitored at 280 nm. Typically, 100 μL of TcOYE sample (or standard mixture) prepared in the aforementioned buffer, at concentration of 1.0 mg mL^{-1}, was applied into aSEC column. The retention times recorded for all standard proteins as well as TcOYE were transformed into the partial coefficient applying the following equation:

$$k_{av} = \frac{V_e - V_0}{V_t - V_0} \quad (1)$$

where V_e is the elution volume of the protein; V_0 is the void volume of the column and the V_t is the total volume of the column. The -log k_{av} was plotted against the R_s in order to estimate the R_s of the TcOYE by liner regression.

2.7. Analytical ultracentrifugation

Analytical ultracentrifugation (AUC) experiments were performed in a Beckman Optima XL-A analytical ultracentrifuge. Sedimentation velocity experiments for TcOYE were carried out in six concentrations, ranging from 0.1 to 0.7 mg mL^{-1} prepared in 25 mM Tris–HCl (pH 8.0) containing 100 mM NaCl and 1 mM β-mercaptoethanol. The measures were performed at 20 °C, 35,000 rpm (AN-60Ti rotor), and data collection were performed at 234 or 239 nm, for the 3 lowest and 3 highest TcOYE concentrations, respectively. The experimental data were fitted by the SedFit software (Version 11.8) [17]. The frictional ratio (f/f_0) parameter was used as a regularization parameter and was allowed float freely. The experimental sedimentation coefficients (s) were found as the maximum of the peaks of the c(S) distribution curves. The apparent s-value was used to calculate the standard sedimentation coefficient at 0 mg mL^{-1} of protein concentration ($s^0_{20,w}$), an intrinsic parameter of the particle [18]. The SedFit software estimated the standard sedimentation coefficients ($s_{20,w}$) since we supplied the buffer viscosity ($\eta = 1.0185 \times 10^{-2}$ poise), buffer density ($\rho = 1.00307$ g mL^{-1}) and partial-specific volume ($V_{bar} = 0.7342$ mL g^{-1}), estimated by the Sednterp program. The $s^0_{20,w}$ was calculated by linear regression of the curve of the $s_{20,w}$ by protein concentration. The f/f_0 was calculated by the ratio of the sedimentation coefficient of a sphere of the same mass as the experimental one.

The molecular mass (MM) of TcOYE in solution was obtained from the global fitting, using the "Species Analysis" model of the SEDPHAT program (v. 8.2). For that, the 6 data sets obtained from the sedimentation velocity experiments at different protein concentrations were uploaded to the SEDPHAT program [19]. In this analysis, all parameters were allowed to float freely followed by mathematical analysis. The statistical method used was the "Monte-Carlo non-linear regression" with at least 100 interactions and confidence level of 0.68.

2.8. Small angle X-ray scattering

SAXS experiments were performed at the D02A-SAXS2 beamline at the Brazilian Synchrotron Light Laboratory (LNLS, Campinas-SP, Brazil). The X-ray scattering data were recorded (two consecutive frames of 300 s) using a two-dimensional position-sensitive MARCCD detector. The measurements were performed with a monochromatic X-ray beam ($\lambda = 1.488$ Å) at two different sample-to-detector distances: ~2400 and ~550 mm, covering a scattering vector range of 0.01 $Å^{-1} < q < 0.55$ $Å^{-1}$, where q is the magnitude of the q-vector defined as $(4\pi/\lambda)\sin\theta$ (where 2θ is the scattering angle). Furthermore, the scattering intensity from the buffer solution was subtracted, considering the sample's X-ray absorption. SAXS measurements were carried out with TcOYE samples at 3.4 and 1.7 mg mL^{-1} in 25 mM Tris–HCl (pH 8.0) with 100 mM NaCl. The effect of ligands on the TcOYE structure conformation was also monitored by SAXS. Menadione (Sigma) and β-lapachone (Sigma), at a concentration of 350 μM and 500 μM, respectively, were incubated with TcOYE (1.7 mg mL^{-1}) in the buffer described above containing 10% of dimethyl-sulfoxide (DMSO). The effect of 10% of DMSO on the structure of TcOYE was also tested as control. Fresh stock solution of menadione and β-lapachone were prepared in 100% of DMSO. Phenazine (Sigma) was also tested at 700 μM in the aforementioned buffer without DMSO. SAXS data were obtained at two independent experiments and at different protein concentrations to avoid aggregation effects (data not shown).

As described by Guinier's law [20], the scattering intensity, $I(q)$, in the small q-range, can yield the scattering particle radius of gyration, R_g, and the forward scattering intensity, $I(q \rightarrow 0)$, is related to the protein MM [21,22]. Besides, the Porod's volume was calculated by the Primus program [23]. Furthermore, a Fourier transform connects $I(q)$ to the pair distance distribution function, $p(r)$, which provides information about the protein shape and maximum dimension (D_{max}) [20,24].

The $p(r)$ functions were evaluated by the GNOM software [25] and in addition to the D_{max} value, this program also provided the forward scattering intensity value, $I(q \rightarrow 0)$ [22,26]. The GENFIT software was used to calculate the protein form factor, which uses the protein crystallographic structure as previously described [27–29]. This methodology allows calculating the theoretical protein scattering curve, assuming that the structure of the protein in solution is the same found in the crystallographic structure.

The GASBOR program [30] was used to generate *ab initio* models for TcOYE based on the SAXS data. As *ab initio* modeling approach does not provide a unique solution, 10 independent *ab initio* reconstructions were performed and then averaged using the DAMAVER program package [31]. Each of these *ab initio* models, before being merged by the DAMAVER package, was analyzed by the HydroPro software in order to predict its hydrodynamic properties [32]. This analysis allowed to compare the predicted hydrodynamic properties of the 10 *ab initio* models to the experimental data obtained here. The crystallographic model determined for TcOYE was analyzed by the HydroPro software.

2.9. Molecular docking simulations

β-lapachone, menadione and phenazine were used as ligands for molecular docking simulations with TcOYE. The ligand structure and geometric parameters were calculated with the GlycoBioChem PRODRG2 Server program [33]. AutoDock Vina [34] was used for molecular docking simulations using a radius of 15 Å from the FMN prosthetic group as the binding site. To increase the accuracy of the results, 10 consecutive runs were performed and the top ranked score from each run was used to calculate the average score for each ligand pose. The top ranked pose was then submitted to a molecular dynamics simulation of 10 ns on YASARA, using YAMBER3 force field [35] and explicit solvation. The binding energy was calculated throughout the entire simulation considering the potential and solvation energies for the complex, receptor and ligand. Electrostatic surface calculations were carried out with APBS [36], atomic interactions are displayed in PoseView 2D format [37].

3. Results and discussion

3.1. Cloning, expression, purification and spectroscopic characterization

The encoding DNA of TcOYE, cloned into the pET28a expression vector, was expressed in *E. coli* BL21(DE3) cells. The His-tagged protein was highly expressed in the soluble fraction (Fig. 1A: lane 5) and purified to homogeneity by affinity chromatography (Fig. 1A: lane 6). The His-tag at the N-terminus was removed by limited proteolysis with thrombin and the cleaved sample was further purified by size-exclusion chromatography (Fig. 1A: lane 7). Circular dichroism spectropolarimetry was used to assess the TcOYE secondary structure content (Fig. 1B), pointing out that TcOYE was obtained in the folded state.

3.2. High-resolution crystal structure

TcOYE was crystallized in two crystalline forms $P2_12_12_1$ and $P2_1$ and diffraction data were collected to a maximum resolution of 1.27 and 2.00 Å, respectively. The refinement converged to crystallographic residuals of 14.6% (R_{free} 17.0%) and 19.4 (R_{free} 24.2%) for $P2_12_12_1$ and $P2_1$ crystalline forms, respectively. In the $P2_12_12_1$ crystalline form, one TcOYE molecule is found in the asymmetric unit, whereas in the $P2_1$ space group, four protomers are found, suggesting that TcOYE could assume some oligomeric form. The final models displayed excellent overall stereochemistry with low RMSD values and most residues (>96.5%) situated in favored regions of the Ramachandran plot (Table 1).

TcOYE displays a canonical $(\alpha/\beta)_8$-barrel fold with a FMN prosthetic group located at the large active-site cavity (Fig. 2A and B). TcOYE also possesses characteristic extra barrel elements, including (i) the N-terminal β-hairpin (residues 10–19) that closes the bottom of the barrel, (ii) the capping subdomain (105–164), which participates in the formation of the large active-site pocket (see below), (iii) the α-helical motif (196–222) related to substrate recognition, and (iv) the "inner" α-helix (336–341) that contributes to FMN binding (Fig. 2A).

Structure comparisons of TcOYE with other structurally characterized OYEs from *Solanum lycopersicum* (SlOYE – 1.09 Å r.m.s.d over 339 Cα atoms – PDB code: 1ICP), *Shewanella oneidensis* (SoOYE – 1.4 Å r.m.s.d over 348 Cα atoms – PDB code: 2GOU) and *Burkholderia pseudomallei* (BpOYE – 1.24 Å r.m.s.d over 341 Cα atoms – PDB code: 3GKA) revealed a very conserved structural architecture with only significant differences in the capping subdomain and in the loop between β6 and α6 elements (Fig. 2C). All catalytically relevant residues and the prosthetic group-binding site are fully conserved. The most divergent region among these OYEs is the extended loop (118–129), which can vary in length and composition changing the volume and accessibility to the active site (Fig. S1). The loop 141–156 of the capping subdomain, in TcOYE as well as in orthologous OYEs is intrinsically flexible exhibiting high B-factor values (Fig. 2C) [9].

3.3. The active site

Using the high-resolution structure at 1.27 Å, it was possible to depict a detailed binding mode of the FMN prosthetic group (Fig. 2D). The isoalloxazine ring is accommodated in a hydrophobic pocket adjacent to the capping subdomain, which is surrounded by the residues

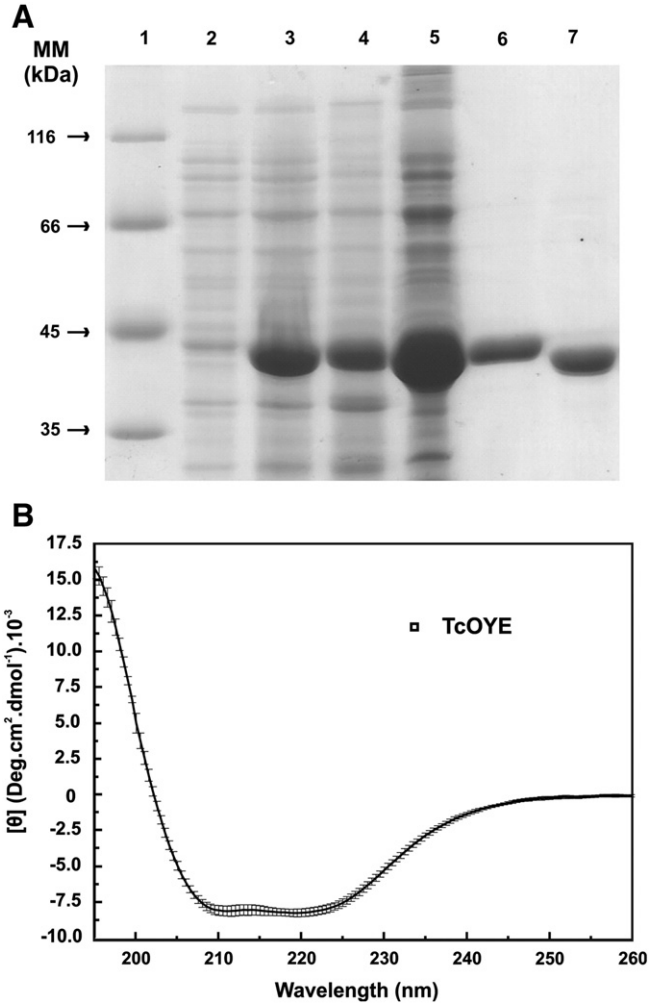

Fig. 1. TcOYE expression, purification and circular dichroism analysis. A) SDS-PAGE showing the expression and purification of TcOYE. Lane 1 represents the MM markers; Lanes 2 and 3 are, respectively, the non-induced and induced cells; Lanes 4 and 5 are the pellet and the supernatant of the lysed cells; Lane 6 is the eluted fraction of the nickel affinity chromatography and Lane 7 is the fraction of the size exclusion chromatography after digestion of the His-tag with thrombin (see the Material and methods section for details). B) Mean residue ellipticity [θ] of TcOYE (3 to 35 μM) was measured from 195 up to 260 nm in 25 mM Tris–HCl (pH 8.0) with 100 mM NaCl and 1 mM β-mercaptoethanol at 20 °C and in a 0.2 and 1.0 mm pathlength cell. The presented spectrum is an average of 4 spectra, after normalization, collected at different protein concentrations. This data suggested that TcOYE was purified in the folded state.

Table 1
Data collection and refinement statistics.

	Crystalline form I	Crystalline form II
Data collection		
Space group	$P2_12_12_1$	$P2_1$
Unit cell parameters (Å,°)	$a = 57.35$, $b = 68.66$ and $c = 85.19$	$a = 50.77$, $b = 118.47$ and $c = 111.12$ $\beta = 90.089$
Resolution	30.00–1.27 (1.32–1.27)	40.00–2.00 (2.07–2.00)
No. unique reflections	87,922 (8818)	80,586 (8820)
Multiplicity	4.9 (4.6)	3.9 (4.0)
Completeness (%)	99.9 (98.3)	99.9 (90.9)
R_{merge} (%)	4.7 (52.2)	6.9 (25.1)
I/σ(I)	28.7 (2.7)	14.9 (5.3)
Refinement		
R_{work}/R_{free} (%)	14.6/17.0	19.4/24.2
Average B-factor	14.68	24.69
r.m.s.d. for bond lengths (Å)	0.005	0.014
r.m.s.d. for bond angles (°)	1.161	1.645
Protein chain	1	4
Water molecules	363	469
Ligand molecules	7 (1 FMN, 3 GOL and 3 PEG)	8 (4 FMN and 4 DMS)
Ramachandran plot		
Favored region (%)	97.61	96.7
Outlier region (%)	0.27	0.53
PDB entry code	4E2B	4E2D

FMN: Flavin mononucleotide.
GOL: Glycerol.
DMS: Dimethyl sulfoxide.

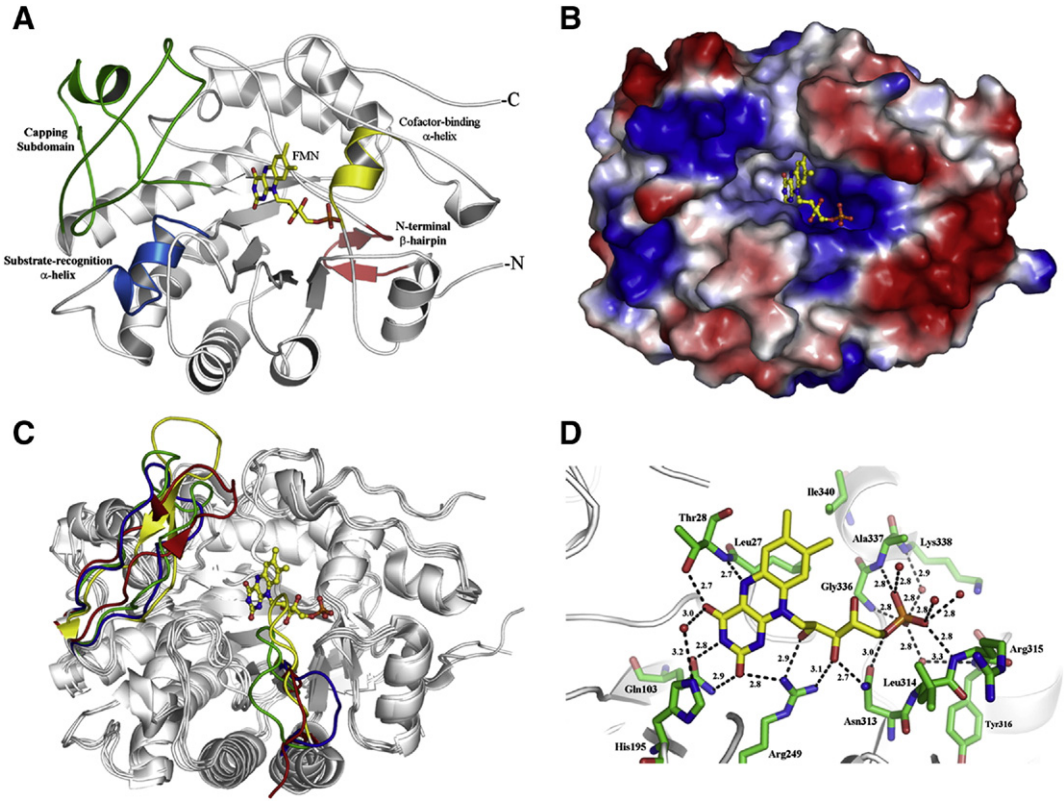

Fig. 2. TcOYE structural analysis. A) Overall fold highlighting the extra barrel elements and the FMN prosthetic group. B) Electrostatic surface representation with the FMN molecule bound to the active-site pocket. The positively charged regions are indicated in blue and the negatively charged regions are indicated in red. C) Structural superposition of TcOYE structure (green) on OYEs from *Burkholderia pseudomallei* (blue), *Shewanella oneidensis* (yellow) and *Solanum lycopersicum* (red). The structurally distinct regions are colored according to the protein. D) A zoom of the FMN binding site showing all contacts established between TcOYE and FMN.

Ala^{25}, Pro^{26}, Leu^{27}, Thr^{28}, Ala^{61}, Gln^{103}, His^{195}, Arg^{249}, Tyr^{363} and Tyr^{364}. The O_4 atom of the isoalloxazine ring is hydrogen bonded to Thr^{28}O, Thr^{28}O$^{\gamma1}$ and Ala^{61}O atoms, whereas the O_2 atom makes polar contacts with Gln^{103} and Arg^{249} side chains. Gln^{103} also interacts with the N3 atom of the isoalloxazine ring. The hydroxylated medial region is strongly attached to the Arg^{249} guanidinyl group and additionally to Asn^{313} and water-mediated contacts. The tail region, comprising the phosphoryl group, is stabilized by the amide groups of the N-terminal region of the "inner" α-helix, the Arg^{315} main chain and a cluster of solvent molecules. Curiously, the Arg^{315} side chain is flexible in the TcOYE structure and does not participate in the phosphoryl moiety coordination, as observed for other OYEs' structures. In the BpOYE structure, there is an Asn residue at the corresponding position, which makes a water-mediated interaction with the phosphoryl group. In both SoOYE and SlOYE structures, the side chain of the Arg^{337} (TcOYE numbering) makes a salt bridge with the tail portion of FMN.

Biologically, TcOYE can metabolize several kinds of compounds with different sizes, from small compounds, such as menadione, phenazine and β-lapachone [6,9], to large compounds such as komaroviquinone [5], 12-oxophytodionate, a PGH_2 substrate analog [10], as well as NAD(P)H that works as coenzyme. The ability to handle with such diversity of ligands originates from a large and plastic active site. The TcOYE active site is surrounded by two flexible structures: the capping subdomain (mainly the loop 141–156) and the C-terminal loop (residues 360–368) (Fig. 2C). The C-terminal loop contributes with two tyrosine residues that stabilize the FMN conformation. The loop 141–156 of the capping subdomain can act as a gate for entering or releasing of substrates or can participate in substrate selection (see below). Another possibility is the involvement of the capping subdomain in the catalytic mechanism of OYEs, however the conservation degree of the capping subdomain is too low to support this hypothesis (Fig. S1).

3.4. TcOYE behaves as a globular monomer in solution

In order to analyze possible oligomeric states of TcOYE in solution, we performed aSEC and sedimentation velocity AUC experiments. Fig. 3A shows chromatograms of TcOYE and standard proteins of known R_s, suggesting that TcOYE has a homogeneous size distribution in solution. The TcOYE R_s was estimated to be 27 ± 2 Å by linear regression (Fig. 3A, inset) and from this value; we estimated f/f_0 of about 1.17 ± 0.08, indicating that TcOYE behaved as a globular protein.

Fig. 3B shows the continuous c(S) distribution obtained for TcOYE from AUC experiments, at three protein concentrations, which also indicated a monodispersive state. TcOYE presented a $s^0_{20,w}$ of about 3.60 S (Fig. 3B, inset) and a f/f_0 of about 1.21 (Table 2), which corresponds to a globular monomer. Using the SEDPHAT software, we also performed a global analysis of the sedimentation velocity data set and obtained a MM of about 43 kDa, which strongly supported the monomeric form of TcOYE in solution, although tetramer (PDB code: 4E2D) and dimer (PDB code: 3ATY) [9] were observed in crystalline structures. All these evidences enable us to conclude that TcOYE is a globular monomer in solution.

3.5. TcOYE solution structure differs from crystalline form

SAXS experiments were performed in order to improve the understanding of TcOYE behavior in solution in the absence and presence of ligands. Fig. 4A shows the scattering curve of TcOYE at 3.4 mg mL^{-1} in 25 mM Tris–HCl (pH 8.0) with 100 mM NaCl (*open circles*), along

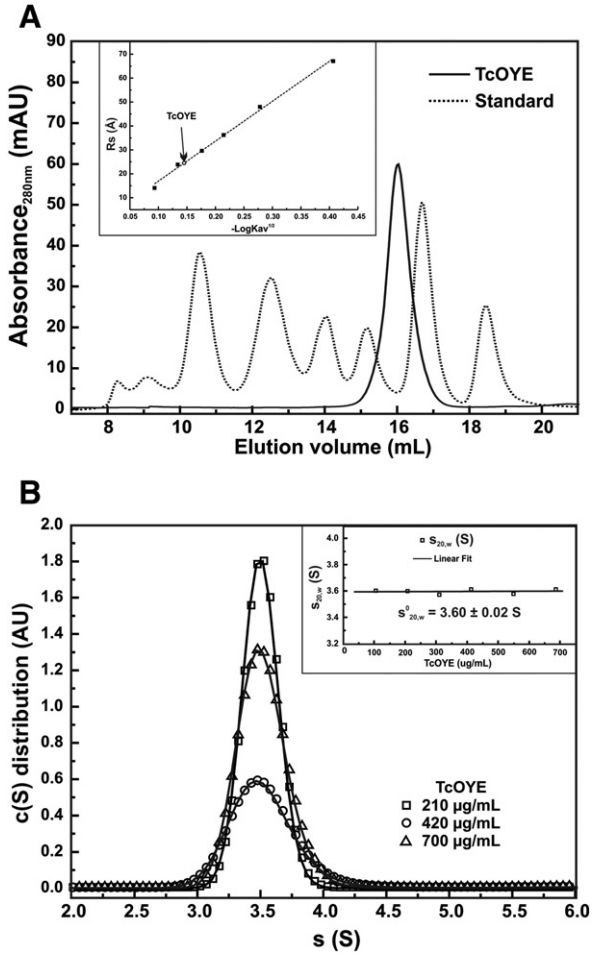

Fig. 3. TcOYE is a globular monomer in solution. A) aSEC experiments (see the Material and methods section for details) suggested that TcOYE eluated between ovalbumin and carbonic anhydrase. *Inset:* the arrow shows the partition coefficient of TcOYE which correspond to a R_s of 27 ± 2 Å. B) The continuous c(S) distributions calculated from the sedimentation velocity AUC experiments where the maximum of peaks resulted in the $s_{20,w}$. The figure displays experiments in 0.21, 0.42 and 0.70 mg mL^{-1} of TcOYE in 25 mM Tris–HCl (pH 8.0) containing 100 mM NaCl and 1 mM β-mercaptoethanol, obtained in 236 nm (0.21 mg mL^{-1}) and 239 nm (0.42 and 0.70 mg mL^{-1}). *Inset*: Plot of $s_{20,w}$ versus protein concentration which was fitted by linear regression in order to calculate the $s^0_{20,w}$ of 3.60 ± 0.02 S. The results suggested that TcOYE behaves as a globular monomer in solution (see text for details).

with the regularization fitting using the GNOM software (*black line*). The Guinier plot exhibited a linear profile, indicating satisfactory monodispersity of TcOYE samples (Fig. 4A—inset). This analysis also indicated that the protein R_g and I(0) were equal to 22.2 ± 0.2 Å and 0.0235 ± 0.003 cm^{-1} mg^{-1} mL, respectively. The I(0) value calculated corresponds to a MM of 41 ± 5 kDa (Table 2), supporting the monomeric state at the concentration range studied (~3.4 mg mL^{-1} or ~40 μM). The hydrated volume estimated from SAXS data, through Porod's law, was similar to that calculated for a hydrated particle of 43 kDa and also similar to that value estimated for the crystalline form, corroborating to the TcOYE monomeric state in solution (Table 2).

Comparisons of the theoretical scattering curve calculated from TcOYE crystallographic atomic coordinates with experimental SAXS data showed significant differences between in solution and crystalline states (Fig. 4A). Fig. 4B depicts the calculated $p(r)$ function for TcOYE SAXS data and compared it with the theoretical curve obtained from crystallographic structure (Fig. 4B, *red line*). The $p(r)$ functions have different D_{max} values, being equal to 80 ± 5 and 60 ± 2 Å, for experimental and theoretical fitting, respectively. Nevertheless, it should be noticed that the maximum in $p(r)$ functions are similar and around 30 Å. These observations indicated that the protein has slightly different structures in solution and crystalline states. In addition, it is also interesting to observe that the theoretical R_g for the crystallographic model, evaluated by both GENFIT and HydroPro programs, were also slightly lower than the experimental data (Table 2), suggesting that the crystallographic structure is somewhat more compact than that in solution. Altogether, these data indicate that TcOYE in solution exhibits characteristics of globular particle, but it also has a slightly more elongated structure in comparison to the crystallographic structure.

The TcOYE *ab initio* model was reconstructed based on the SAXS data using the routine implemented by the GASBOR program [30]. The hydrodynamic parameters, such as $s_{20,w}$ and R_s, estimated for the TcOYE *ab initio* models were very similar to the experimental data (Table 2). However, the structural properties calculated for the *ab initio* models, like R_g, hydrated volume and D_{max}, were slightly higher than the experimental data as well as estimated for the crystalline form (Table 2). These results were expected since the *ab initio* models behave as a single shape representation and exhibit hydrodynamic and structural properties that do not consider intrinsic flexibility. Despite that, the *ab initio* models were merged using the DAMAVER package and the averaged model is presented in Fig. 4C. The normalized spatial discrepancy (NSD) value observed for the *ab initio* models, used by the DAMAVER, was of 0.50 ± 0.05 showing the overall quality of individual

Table 2
Structural properties determined to TcOYE in solution and comparison to those predicted to the crystallographic structure.

Technique/methodology		*TcOYE* hydrodynamic and structural properties							
		MM (kDa)	$s^0_{20,w}$ (S)	Rs (Å)	f/f_0	R_g (Å)		D_{max} (Å)	V ($\times 10^{-3}$ Å^3)
						Guinier	GNOM		
Predicted for a sphere[a]		43.0	4.35	23	1.0	–	–	–	68[g]
AUC/aSEC		43.1 ± 0.5[b]	3.60 ± 2[c]	27 ± 2	1.21 ± 0.01[d]	–		–	–
SAXS	Native	41 ± 5	–	–	–	22.2 ± 0.1	22.7 ± 0.3	80 ± 5	70 ± 2[e]
	Phenazine	42 ± 5	–	–	–	22.0 ± 0.1	22.8 ± 0.3	80 ± 5	65 ± 4[e]
	DMSO	42 ± 6	–	–	–	22.8 ± 0.1	22.3 ± 0.4	75 ± 5	69 ± 3[e]
	β-lapachone	40 ± 6	–	–	–	22.4 ± 0.1	22.6 ± 0.3	80 ± 5	67 ± 4[e]
	Menadione	43 ± 5	–	–	–	22.0 ± 0.1	22.6 ± 0.2	70 ± 5	67 ± 3[e]
GENFIT (crystalline form)		–	–	–	–	21.0 ± 0.5		60 ± 2	–
HydroPro[f]	Crystalline form	–	3.69 ± 0.03	27 ± 2	1.18 ± 0.02	20.6 ± 0.4		68 ± 2	70 ± 2
	Ab initio model	–	3.46 ± 0.03	29 ± 2	1.25 ± 0.02	24.8 ± 0.8		90 ± 10	80 ± 2

[a] Values predicted for *TcOYE* as a globular monomers in water and 20 °C (predicted by Sednterp software).
[b] Calculated from SedPhat global fitting of the sedimentation velocity data.
[c] Data extrapolated for water, 20 °C and 0 mg mL^{-1} of protein[18].
[d] Average data from f/f_0 supplied by the fitting of the sedimentation coefficient data by SedFit. The ratio of the predicted s for a sphere and experimental $s^0_{20,w}$ also yields a f/f_0 of same value.
[e] Estimated from Porod's law.
[f] Obtained from the TcOYE crystallographic structure and from the TcOYE *ab initio* model (data predicted for water and 20 °C).
[g] Volume estimation based on V_{bar} and MM relationship, considering a hydration of 0.3 g/g.

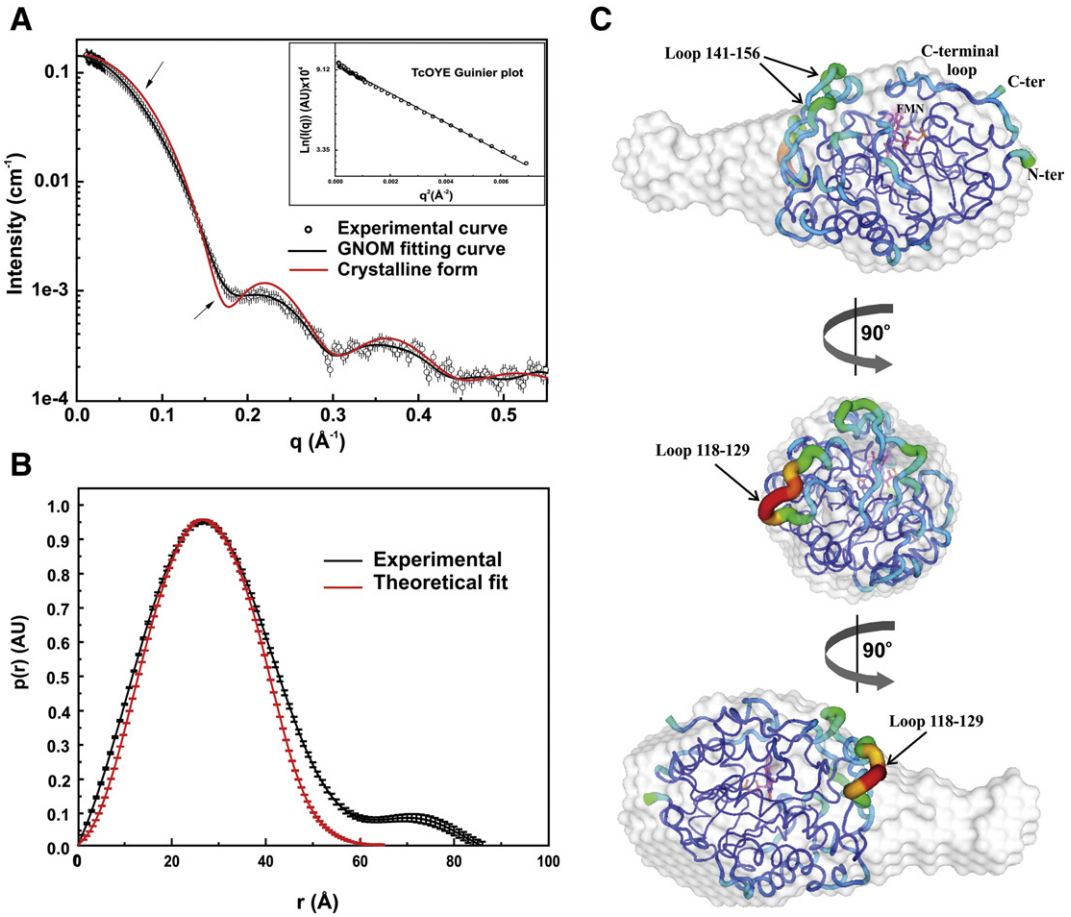

Fig. 4. TcOYE solution structure is slightly different from the crystallographic structure. A) Scattering curve of TcOYE 3.4 mg mL^{-1} in the presence of 25 mM Tris–HCl (at pH 8.0) containing 100 mM NaCl (open spheres). The *solid black line* represents the best fitting obtained with the GNOM software. The *solid red line* represents the theoretical scattering curve obtained to the crystallographic structure of the TcOYE. B) Experimental $p(r)$ function obtained to the TcOYE (*black line*) presents a Gaussian shape until 60 Å and frequencies of distance distribution until 85 Å, emphasizing its D_{max} and a slightly elongated shape. The theoretical $p(r)$ function generated to the crystallographic structure (*red line*) has a Gaussian form suggesting the globular shape of TcOYE. See text for details. C) *Ab initio* model generated for TcOYE superposed with the crystallographic structure (PDB acc. no. 4E2B). The *ab initio* model suggested that TcOYE possesses an elongated shape, which is not observed for the crystallographic structure (see text for details). The crystalline structure is colored and thickness according to the B-factor. The loops 141–156 and 361–368 are located at the top of the substrate binding site and might open due to their flexibility and dynamics, which increase the TcOYE dimension in solution (see text for details).

reconstructions. As expected by the analysis of the $p(r)$ function (Fig. 4B), TcOYE *ab initio* model has a slightly elongated shape, with maximum dimension of around 90 Å (Table 2). The crystallographic structure showed a good agreement with the SAXS envelope; however, the SAXS model indicates an extended form that is not observed in the crystal data (Fig. 4C).

Analysis of TcOYE atomic coordinates and B-factor values (as argued above) suggests that two long surface loops consisting of the capping subdomain (residues 105–164) and C-terminal loop (residues 352–378) (Figs. 2C and 4C) could be involved in the structural differences between in solution and crystal forms. These two regions together contain 22% of all TcOYE amino acids and its dynamics or flexibility should affect the X-ray scattering of the solution structure. To test this hypothesis, we modeled the loop 141–156 of the capping subdomain and the C-terminal loop, separately, as flexible entities through the Ensemble Optimization Method (EOM) [38]. Both approaches led to adequate fittings with the SAXS experimental data (Fig. S2) suggesting that the TcOYE inherent flexibility of these surface loops is related to the extended conformation observed in SAXS experiments. As TcOYE has more loops and regions on its surface (for instance the extended loop 118–129—Fig. 4C), which may contribute for the intrinsic flexibility, we cannot point the regions responsible for the flexibility through the EOM routine. Besides, the TcOYE was submitted to limited proteolysis with proteinase K which led to the formation of four stable fragments (~35 kDa, ~26 kDa, ~18 kDa and ~7 kDa) suggesting that TcOYE has flexible segments on its structure (Fig. S3). These fragment sizes are consistent with proteinase K proteolysis on the TcOYE flexible loops (as indicated above) corroborating to the hypothesis that the protein flexibility is responsible for the enlarged dimensions observed in the SAXS experiments.

Furthermore, it is important to note that TcOYE crystallographic structure has several additional loops on its surface, which can also contribute to the protein flexibility or global "breathing". Taken all together, the protein flexibility and dynamics can lead both D_{max} and R_g to slightly higher values than those estimated for the crystallographic structure. Our *ab initio* model, which is a single shape structure representation, has enlarged dimensions as well as similar predicted hydrodynamic properties to the experimental data (Table 2), indicating the presence of flexibility. Probably due to the crystal packing effects, the flexible loops adopt a partially ordered conformation decreasing the dimensions of the crystallographic structure.

3.6. Binding mode and the effects of naphthoquinones on TcOYE structure

In order to understand the specificity and binding mode of naphthoquinones to TcOYE, an *in silico* and in solution investigation

were carried out with β-lapachone, menadione and phenazine. Particularly the natural compound β-lapachone [11] works as substrate for TcOYE, which forms a semiquinone radical anion and acts as a weak inhibitor of the PGF2α synthase activity of TcOYE [6]. It has also been implicated in superoxide anion and hydrogen peroxide productions in *T. cruzi* cells [39,40], which is trypanocidal [41].

The tested compounds were successfully docked in the binary TcOYE–FMN complex (Fig. S4) and bounded to a positively charged pocket surrounded by the isoalloxazine ring of FMN (Figs. 5A and S5). All ligands are stabilized by π–π interactions between the flavin moiety and the naphthoquinone ring. β-lapachone additionally makes interactions with hydrophobic (Phe^{71} and Met^{290}) and polar (His^{195} and Tyr^{200}) protein residues. The O^{AD} atom is hydrogen bonded to both His^{195} and Tyr^{200}, and Phe^{71} and Met^{290} make carbon–carbon interactions with β-lapachone cyclic carbon atoms (Fig. 5B). Besides, menadione makes hydrogen bond with His^{195} as well Asn^{198} and Thr^{28} (Fig. 5D). These residues were also shown to be critical for interacting with menadione [9] and p-hydroxybenzaldehyde [10]. Phenazine adopted distinct orientations within the active-site pocket, despite in all poses the π–π interactions are maintained (Fig. S5). This behavior is explained by the lack of hydrogen bonds to orientate the ligand in a specific configuration since there is no hydroxyl groups attached to the phenazine naphthoquinone ring such as in β-lapachone and menadione.

In addition, the effects of β-lapachone, phenazine and menadione on the TcOYE structure were investigated by SAXS technique. It was expected that the flexible region encompassing the capping domain could become structured upon ligand binding, altering the overall structural properties of the protein detected by SAXS. In fact, docking studies suggest that the $Tyr^{147}$and Phe^{148} of the loop 141–156 of the capping subdomain may interact with the carbonic chain of the 12-oxophytodionate, an PGH_2 substrate analog, taking it to a closed conformation [10]. Nevertheless, SAXS measurements indicate that the overall structure of TcOYE did not change after phenazine, menadione or β-lapachone were added to the solution (Fig. S6). Even the calculated R_g (from Guinier's law—Fig. S6A) and the hydrated volumes for TcOYE in the presence of ligands were similar (inside the error) to that in the absence of ligands (Table 2). The *p(r)* functions in the presence of phenazine, menadione and β-lapachone are similar and present similar D_{max}-values (inside the error—Table 2) to that observed for the protein in the absence of ligands (Fig. S6B). Altogether, the SAXS curves suggested that TcOYE has an elongated conformation even in the presence of ligands and such structure is quite similar to that one in the absence of ligands. Thus, the presence of known ligands of TcOYE did not result in a more compact structure as expected, at least not detectable by SAXS. Based on this observation, two possibilities can be indicated: 1) the interaction with ligands did not change the overall TcOYE solution structure or 2) the ligands used in the SAXS experiments do not interact with the flexible loops.

Analyzing the TcOYE–FMN ternary complexes obtained by molecular docking simulations we can observe that β-lapachone, menadione and phenazine are positioned more than 4 Å far from both $Tyr^{147}$and Phe^{148} of the capping subdomain, suggesting that these residues do not participate in the interaction with small TcOYE ligands. Since TcOYE can act on a broad range of molecules with distinct sizes, the loop 141–156 of the capping domain may participate and interact only with large compounds, which could result in a more compact conformation in solution, as observed in crystallographic structures. We hypothesize that the loop 141–156 of the capping subdomain as well as the C-terminal loop (residues 360–368) can present the lid mechanism where they assume a flexible or open conformation to allow the substrate binding/release in the active site.

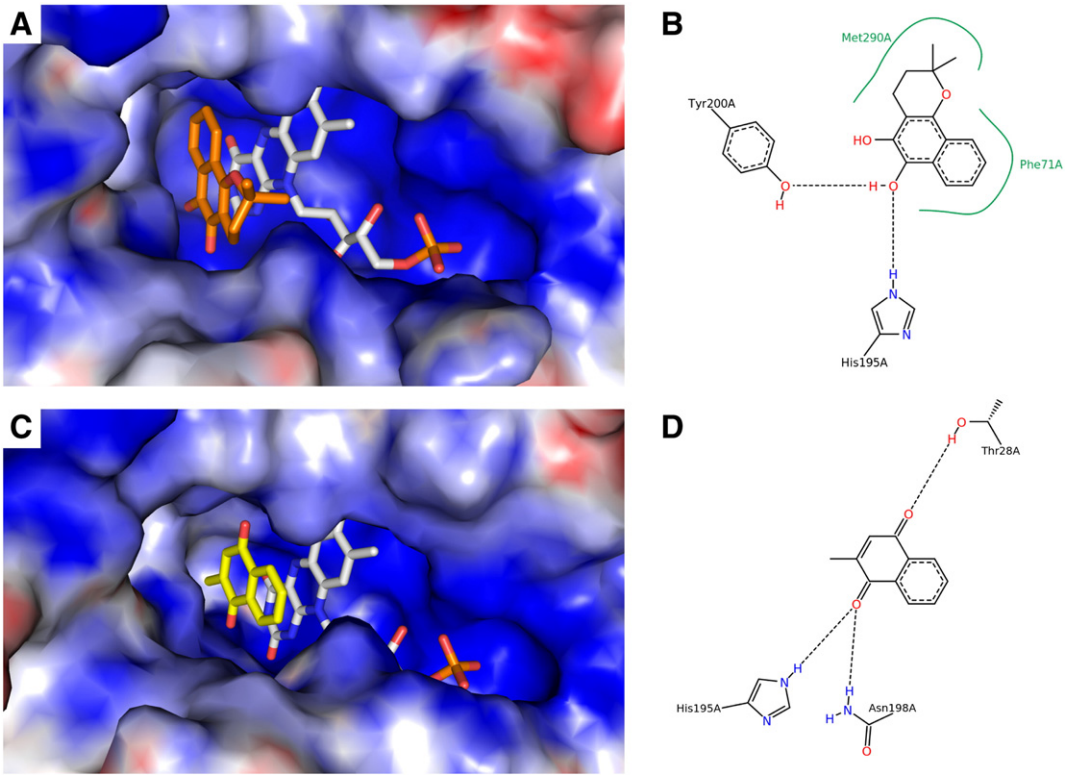

Fig. 5. Molecular dynamics simulation of the ternary complexes β-lapachone/FMN/TcOYE and menadione/FMN/TcOYE. Electrostatic surface representation of TcOYE active-site pocket with the docked β-lapachone (A) and menadione (C) (carbon atoms in orange and yellow, respectively) and the FMN prosthetic group (carbon atoms in white). The positively charged regions are indicated in blue and the negatively charged regions are indicated in red. 2D map showing β-lapachone/TcOYE (B) and menadione/TcOYE (D) interactions. Dotted lines are hydrogen bonds and green curves represent hydrophobic contacts.

4. Concluding remarks

TcOYE is an important oxidoreductase involved in the metabolism of trypanocidal drugs and its detailed characterization is instrumental for a better understanding of parasite metabolism and may help in the development of new strategies to improve the current chemotherapy. The crystal structure of TcOYE isoform was determined in two high-resolution crystalline forms, enabling a detailed analysis of the FMN binding mode and other intrinsic properties like the flexible region in the capping subdomain and the highly solvated active site. Structural comparisons with other OYEs showed a conserved structural scaffold with significant differences in the capping subdomain. This motif may alter the active-site pocket in shape and volume allowing the entrance of large ligands as well as contributing for their binding. On the other hand, small ligands may not require the capping subdomain for binding to TcOYE. Moreover, aSEC and AUC analyses showed that TcOYE is a globular monomer in solution. SAXS data, even in the presence of ligands, showed that TcOYE is predominantly globular, which resembles the crystallographic structure. However, it has a longer molecular envelope in solution when compared to the crystal structure, which was attributed to inherent protein flexibility. Taken together, our study sheds light on the solution behavior of TcOYE by different biophysical approaches and combined with high-resolution crystal structure analysis suggests that the capping subdomain may present an open-close dynamics. TcOYE is responsible for the drug-metabolizing activity of trypanocidal drugs and the detailed knowledge of its structural and functional properties is instrumental for a better understanding of parasite biology and development of new therapies against Chagas' disease.

Acknowledgments

J.C. Borges thanks the FAPESP for financial support (grant #2007/05001-4 and #2011/23110-0) and the CNPq for Research Fellows. We acknowledge the Spectroscopy and Calorimetry Laboratory at Brazilian Biosciences National Laboratory (LNBio/CNPEM-ABTLuS, Campinas, Brazil) for the provision the AUC device. The authors are also in debt with Prof. Paolo Mariani and Francesco Spinozzi, both from the Università Politecnica delle Marche, Ancona, Italy, who gently provided GENFIT software. We also thank the Brazilian Synchrotron Light Laboratory (LNLS/CNPEM-ABTLuS, Campinas, Brazil) for the use of both SAXS and MX2 beamlines.

Appendix A. Supplementary data

Supplementary data to this article can be found online at http://dx.doi.org/10.1016/j.bpc.2013.08.004.

References

[1] J.D. Maya, M. Orellana, J. Ferreira, U. Kemmerling, R. Lopez-Munoz, A. Morello, Chagas disease: present status of pathogenic mechanisms and chemotherapy, Biol. Res. 43 (2010) 323–331.
[2] S.R. Wilkinson, J.M. Kelly, Trypanocidal drugs: mechanisms, resistance and new targets, Expert Rev. Mol. Med. 11 (2009) e31.
[3] S.R. Wilkinson, M.C. Taylor, D. Horn, J.M. Kelly, I. Cheeseman, A mechanism for cross-resistance to nifurtimox and benznidazole in trypanosomes, Proc. Natl. Acad. Sci. U. S. A. 105 (2008) 5022–5027.
[4] J.D. Maya, B.K. Cassels, P. Iturriaga-Vásquez, J. Ferreira, M. Faúndez, N. Galanti, A. Ferreira, A. Morello, Mode of action of natural and synthetic drugs against *Trypanosoma cruzi* and their interaction with the mammalian host, Comp. Biochem. Physiol A 146 (2007) 601–620.
[5] N. Uchiyama, Z. Kabututu, B.K. Kubata, F. Kiuchi, M. Ito, J. Nakajima-Shimada, T. Aoki, K. Ohkubo, S. Fukuzumi, S.K. Martin, G. Honda, Y. Urade, Antichagasic activity of komaroviquinone is due to generation of reactive oxygen species catalyzed by *Trypanosoma cruzi* old yellow enzyme, Antimicrob. Agents Chemother. 49 (2005) 5123–5126.
[6] B.K. Kubata, Z. Kabututu, T. Nozaki, C.J. Munday, S. Fukuzumi, K. Ohkubo, M. Lazarus, T. Maruyama, S.K. Martin, M. Duszenko, Y. Urade, A key role for old yellow enzyme in the metabolism of drugs by *Trypanosoma cruzi*, J. Exp. Med. 196 (2002) 1241–1251.
[7] H.M. Andrade, S.M.F. Murta, A. Chapeaurouge, J. Perales, P. Nirde, A.J. Romanha, Proteomic analysis of *Trypanosoma cruzi* resistance to benznidazole, J. Proteome Res. 7 (2008) 2357–2367.
[8] S.M.F. Murta, M.A. Krieger, L.R. Montenegro, F.F.M. Campos, C.M. Probst, A.R. Avila, N.H. Muto, R.C. de Oliveira, L.R. Nunes, P. Nirde, O. Bruna-Romero, S. Goldenberg, A.J. Romanha, Deletion of copies of the gene encoding old yellow enzyme (TcOYE), a NAD(P)H flavin oxidoreductase, associates with in vitro-induced benznidazole resistance in *Trypanosoma cruzi*, Mol. Biochem. Parasitol. 146 (2006) 151–162.
[9] K. Yamaguchi, N. Okamoto, K. Tokuoka, S. Sugiyama, N. Uchiyama, H. Matsumura, K. Inaka, Y. Urade, T. Inoue, Structure of the inhibitor complex of old yellow enzyme from *Trypanosoma cruzi*, J. Synchrotron Radiat. 18 (2011) 66–69.
[10] N. Okamoto, K. Yamaguchi, E. Mizohata, K. Tokuoka, N. Uchiyama, S. Sugiyama, H. Matsumura, K. Inaka, Y. Urade, T. Inoue, Structural insight into the stereoselective production of PGF2a by Old Yellow Enzyme from *Trypanosoma cruzi*, J. Biochem. 150 (2011) 563–568.
[11] A.V. Pinto, S.L. de Castro, The trypanocidal activity of naphthoquinones: a review, Molecules 14 (2009) 4570–4590.
[12] Z. Otwinowski, W. Minor, [20] in: W.C. Charles (Ed.), Processing of X-ray diffraction data collected in oscillation mod, Methods Enzymol. Macromolecular Crystallography Part AAcademic Press, 1997, pp. 307–326.
[13] A. Vagin, A. Teplyakov, MOLREP: an automated program for molecular replacement, J. Appl. Crystallogr. 30 (1997) 1022–1025.
[14] G.N. Murshudov, A.A. Vagin, E.J. Dodson, Refinement of macromolecular structures by the maximum-likelihood method, Acta Crystallogr. D: Biol. Crystallogr. 53 (1997) 240–255.
[15] P. Emsley, K. Cowtan, Coot: model-building tools for molecular graphics, Acta Crystallogr. D: Biol. Crystallogr. 60 (2004) 2126–2132.
[16] V.B. Chen, W.B. Arendall III, J.J. Headd, D.A. Keedy, R.M. Immormino, G.J. Kapral, L.W. Murray, J.S. Richardson, D.C. Richardson, MolProbity: all-atom structure validation for macromolecular crystallography, Acta Crystallogr. D: Biol. Crystallogr. 66 (2010) 12–21.
[17] P. Schuck, Size-distribution analysis of macromolecules by sedimentation velocity ultracentrifugation and Lamm equation modeling, Biophys. J. 78 (2000) 1606–1619.
[18] J.C. Borges, C.H.I. Ramos, Analysis of molecular targets of mycobacterium tuberculosis by analytical ultracentrifugation, Curr. Med. Chem. 18 (2011) 1276–1285.
[19] J. Vistica, J. Dam, A. Balbo, E. Yikilmaz, R.A. Mariuzza, T.A. Rouault, P. Schuck, Sedimentation equilibrium analysis of protein interactions with global implicit mass conservation constraints and systematic noise decomposition, Anal. Biochem. 326 (2004) 234–256.
[20] G. Fournet and A. Guinier, in: Small angle scattering of X-rays, Translated by C.B. Walker and K.L. Yudowitch, John Wiley & Sons, New York, 1955 pp. 7–78.
[21] E. Mylonas, D.I. Svergun, Accuracy of molecular mass determination of proteins in solution by small-angle X-ray scattering, J. Appl. Crystallogr. 40 (2007) S245–S249.
[22] D. Orthaber, A. Bergmann, O. Glatter, SAXS experiments on absolute scale with Kratky systems using water as a secondary standard, J. Appl. Crystallogr. 33 (2000) 218–225.
[23] P.V. Konarev, V.V. Volkov, A.V. Sokolova, M.H.J. Koch, D.I. Svergun, PRIMUS: a Windows PC-based system for small-angle scattering data analysis, J. Appl. Crystallogr. 36 (2003) 1277–1282.
[24] O. Glatter, O. Kratky, Small Angle X-Ray Scattering, Academic Press Inc. Ltd, New York, 1982, pp. 17–50.
[25] D.I. Svergun, Determination of the regularization parameter in indirect-transform methods using perceptual criteria, J. Appl. Crystallogr. 25 (1992) 495–503.
[26] L.A. Feigin, D.I. Svergun, Structure Analysis by Small-angle X-ray and Neutron Scattering, Plenum Press, New York, 1987, pp. 59–104.
[27] L.R.S. Barbosa, M.G. Ortore, F. Spinozzi, P. Mariani, S. Bernstorff, R. Itri, The importance of protein–protein interactions on the pH-induced conformational changes of bovine serum albumin: a small-angle X-ray scattering study, Biophys. J. 98 (2010) 147–157.
[28] M.G. Ortore, F. Spinozzi, P. Mariani, A. Paciaroni, L.R.S. Barbosa, H. Amenitsch, M. Steinhart, J. Ollivier, D. Russo, Combining structure and dynamics: non-denaturing high-pressure effect on lysozyme in solution, J. R. Soc. Interface 6 (2009) S619–S634.
[29] R. Sinibaldi, M.G. Ortore, F. Spinozzi, F. Carsughi, H. Frielinghaus, S. Cinelli, G. Onori, P. Mariani, Preferential hydration of lysozyme in water/glycerol mixtures: a small-angle neutron scattering study, J. Chem. Phys. 126 (2007) 235101–235109.
[30] D.I. Svergun, M.V. Petoukhov, M.H.J. Koch, Determination of domain structure of proteins from X-ray solution scattering, Biophys. J. 80 (2001) 2946–2953.
[31] V.V. Volkov, D.I. Svergun, Uniqueness of ab initio shape determination in small-angle scattering, J. Appl. Crystallogr. 36 (2003) 860–864.
[32] J.G. de la Torre, M.L. Huertas, B. Carrasco, Calculation of hydrodynamic properties of globular proteins from their atomic-level structure, Biophys. J. 78 (2000) 719–730.
[33] A.W. Schuttelkopf, D.M.F. van Aalten, PRODRG: a tool for high-throughput crystallography of protein–ligand complexes, Acta Crystallogr. D: Biol. Crystallogr. 60 (2004) 1355–1363.
[34] O. Trott, A.J. Olson, AutoDock Vina: improving the speed and accuracy of docking with a new scoring function, efficient optimization, and multithreading, J. Comput. Chem. 31 (2010) 455–461.
[35] E. Krieger, T. Darden, S.B. Nabuurs, A. Finkelstein, G. Vriend, Making optimal use of empirical energy functions: force-field parameterization in crystal space, Proteins 57 (2004) 678–683.
[36] N.A. Baker, D. Sept, S. Joseph, M.J. Holst, J.A. McCammon, Electrostatics of nanosystems: application to microtubules and the ribosome, Proc. Natl. Acad. Sci. U. S. A. 98 (2001) 10037–10041.
[37] K. Stierand, M. Rarey, Drawing the PDB: protein–ligand complexes in two dimensions, ACS Med. Chem. Lett. 1 (2010) 540–545.

[38] M.V. Petoukhov, D. Franke, A.V. Shkumatov, G. Tria, A.G. Kikhney, M. Gajda, C. Gorba, H.D.T. Mertens, P.V. Konarev, D.I. Svergun, New developments in the ATSAS program package for small-angle scattering data analysis, J. Appl. Crystallogr. 45 (2012) 342–350.
[39] R. Docampo, F.S. Cruz, A. Boveris, R.P.A. Muniz, D.M.S. Esquivel, Lipid peroxidation and the generation of free radicals, superoxide anion, and hydrogen peroxide in β-lapachone-treated *Trypanosoma cruzi* epimastigotes, Arch. Biochem. Biophys. 186 (1978) 292–297.
[40] A. Boveris, R. Docampo, J.F. Turrens, A.O.M. Stoppani, Effect of beta-lapachone on superoxide anion and hydrogen-peroxide production in *Trypanosoma cruzi*, Biochem. J. 175 (1978) 431–439.
[41] C. Salas, R.A. Tapia, K. Ciudad, V. Armstrong, M. Orellana, U. Kemmerling, J. Ferreira, J.D. Maya, A. Morello, *Trypanosoma cruzi*: activities of lapachol and α-and β-lapachone derivatives against epimastigote and trypomastigote forms, Bioorg. Med. Chem. 16 (2008) 668–674.